ADVANCED FUNCTIONAL MATERIALS
www.afm-journal.de



# Red, Green, and Blue Light-Emitting Polyfluorenes Containing a Dibenzothiophene-*S,S*-Dioxide Unit and Efficient High-Color-Rendering-Index White-Light-Emitting Diodes Made Therefrom

*Lei Yu, Jie Liu, Sujun Hu, Ruifeng He, Wei Yang,* Hongbin Wu, Junbiao Peng, Ruidong Xia,* and Donal D. C. Bradley**

**A series of blue (B), green (G) and red (R) light-emitting, 9,9-bis(4-(2-ethylhexyloxy)phenyl)fluorene (PPF) based polymers containing a dibenzothiophene-*S,S*-dioxide (SO) unit (PPF-SO polymer), with an additional benzothiadiazole (BT) unit (PPF-SO-BT polymer) or a 4,7-di(4-hexylthien-2-yl)-benzothiadiazole (DHTBT) unit (PPF-SO-DHTBT polymer) are synthesized. These polymers exhibit high fluorescence yields and good thermal stability. Light-emitting diodes (LEDs) using PPF-SO25, PPF-SO15-BT1, and PPF-SO15-DHTBT1 as emission polymers have maximum efficiencies $LE_{max}$ = 7.0, 17.6 and 6.1 cd $A^{-1}$ with CIE coordinates (0.15, 0.17), (0.37, 0.56) and (0.62, 0.36), respectively. 1D distributed feedback lasers using PPF-SO30 as the gain medium are demonstrated, with a wavelength tuning range 467 to 487 nm and low pump energy thresholds (≥18 nJ). Blending different ratios of B (PPF-SO), G (PPF-SO-BT) and R (PPF-SO-DHTBT) polymers allows highly efficient white polymer light-emitting diodes (WPLEDs) to be realized. The optimized devices have an attractive color temperature close to 4700 K and an excellent color rendering index (CRI) ≥90. They are relatively stable, with the emission color remaining almost unchanged when the current densities increase from 20 to 260 mA $cm^{-2}$. The use of these polymers enables WPLEDs with a superior trade-off between device efficiency, CRI, and color stability.**

## 1. Introduction

Polymer light-emitting diodes (PLEDs) have gained tremendous attention due to their broad application prospects in full-color flat-panel electroluminescence (EL) displays, back-lighting sources for liquid-crystal displays and next-generation solid-state lighting sources.[1–4] Developing advanced red, green and blue (RGB) light-emitting polymers is indispensable in taking forward these applications. Polyfluorenes (PFs) are the most attractive blue light-emitting polymers because of high photoluminescence (PL) quantum efficiency, relatively good thermal and electrochemical stability and facile functionalization at the C-9 position of the fluorene unit. In addition, through the introduction of a variety of different functional units into a fluorene-based copolymer backbone, the emission can be tuned across the entire visible spectrum.[5,6] However, the spectral instability arising from fluorenone defect formation seriously degrades color purity in the blue,[7–9] leading to many efforts to address this problem.[10–14] One of the most effective methods has been incorporation of dibenzothiophene-S,S-dioxide (SO) units.[13,14] Perepichka et al. incorporated (3,7-diyl) SO units into oligofluorenes and found no green emission in the PL spectra after thermal annealing in air.[15] Additionally, a series polyfluorene derivatives were synthesized by introducing SO moieties into main chain of polyfluorenes, which exhibited blue light emission with excellent spectral stability.[16a–c] Liu et al. also reported a poly((alkoxyphenyl-substituted)fluorene-co-SO) (PPF-SO) polymer, which showed both high spectral stability and EL efficiency ($LE_{max}$ = 6.0 cd $A^{-1}$). The resulting excellent device performance is attributed to both alkoxyphenyl substitution at the fluorene C-9 position and incorporation of electron-deficient SO units into the backbone; the latter improve electron injection and make charge injection and transport more balanced.[16d] Consequently, the PPF-SO chemical structure has the potential to function as both an efficient blue emitter and as a wide optical gap segment in more complex copolymers where selective incorporation of narrower gap units then allows realization of longer wavelength emissions.

The most commonly used gap-narrowing units are the 2,1,3-benzothiadiazole (BT) and 4,7-dithienyl-BT (variously abbreviated as DTBT, DBT and TBT). The BT unit was first utilized in green emission fluorene-based copolymer light

Dr. L. Yu, Dr. J. Liu, Dr. S. Hu, Dr. R. He, Prof. W. Yang, Prof. H. Wu, Prof. J. Peng
Institute of Polymer Optoelectronic Materials and Devices
State Key Laboratory of Luminescent Materials and Devices
South China University of Technology
Guangzhou 510640, China
E-mail: pswyang@scut.edu.cn
Dr. R. Xia, Prof. D. D. C. Bradley
Department of Physics and Centre for Plastic Electronics
Imperial College London
Prince Consort Road, London SW7 2AZ, UK
E-mail: ruidong.xia@gmail.com; d.bradley@imperial.ac.uk

DOI: 10.1002/adfm.201203675

emitting diode materials by E. P. Woo and colleagues at the Dow Chemical Company.[17] It has subsequently found widespread use in the design of new organic semiconductors for both light emission and energy harvesting (solar cell) applications, with high performance PLEDs reported by a number of groups. For example: i) Wilkinson et al. reported ultrabright ($\geq 6 \times 10^6$ cd m$^{-2}$) pulsed, small area, green emission PLEDs using a blend of 5% poly(9,9-dioctylfluorene-*co*-benzothiadiazole) (F8BT) with 95% poly(9,9-dioctylfluorene) (PFO),[18] ii) Jen et al reported high efficiency PLED copolymers of 9,9-dihexylfluorene and BT, in some cases also adding hole-transporting comonomers,[19] iii) Wang et al. developed novel green-emitting polyfluorenes combining 4,7-diphenyl-BT and F8 units, with PLEDs fabricated from these polymers exhibiting $LE_{max}$ = 5.96 cd A$^{-1}$ and CIE coordinates (0.29, 0.63),[20] and iv) Chung et al. reported PLEDs gravure printed on plastic substrates using the Sumitomo Chemical Company Lumation Green complex-copolymer (based on F8, BT and arylamine units), thereby yielding maximum performance figures of 8.8 lm W$^{-1}$, 5.4 cd A$^{-1}$ and 66 000 cd m$^{-2}$.[21] Efficient green-emitting poly(fluorene-*co*-SO) derivatives were prepared by incorporating the electron-deficient SO moiety and its arylamine-based derivatives into polyfluorene backbone, which showed balanced electron and hole injection and transportation with $LE_{max}$ attained 9.0 cd A$^{-1}$.[16e] Saturated red-light-emitting co-polyfluorenes were also synthesized first by the Dow Chemical Company,[17] using F8, BT, arylamine and TBT units; Dow Red F[22–24] and more recent proprietary Lumation Red materials are examples. Hou et al. subsequently demonstrated efficient saturated red PLEDs using co-polyfluorenes with F8 and 4,7-di(4-hexylthien-2-yl)-BT (DHTBT) units; $LE_{max}$ = 1.45 cd A$^{-1}$ and CIE coordinates (0.66, 0.34) were achieved.[25] Single white-emitting copolymers based on PFSODPABT were synthesized by introducing a small amount of narrow band-gap emitter bisphenylamine-BT (DPABT) to poly(fluorene-*co*-SO) backbone, which showed slow efficiency roll-off at high current density.[16f]

Recently, the power efficiencies (PE) of the most efficient white PLEDs (WPLEDs) have outperformed those of incandescent lamps,[26,27] suggesting that the replacement of traditional white-light sources with WPLEDs could offer an energy saving opportunity. Several different ways have been reported to realize such devices, the simplest of which use blends of R, G and B polymers as the emission medium.[26–35] Light sources for industrial application need not only to be energy efficient but also to have excellent color stability and a large color rendering index (CRI). Generally, for a high-quality white light source the CRI, which measures how true the color of an object appears when illuminated by that source, should exceed 80 (on a scale from 0 to 100). Unfortunately, many of the WPLEDs reported to exhibit impressive EL efficiencies suffer from strong voltage-dependent color shifts and/or low CRI values, thereby limiting their practical use.[32,34,36,37] Conversely, some other WPLEDs with high color stability have unsatisfactory EL efficiency.[38,39] The simultaneous optimization of WPLED efficiency, color stability and CRI remains an important target.

Here, we report the synthesis and characterization of novel PPF-SO, PPF-SO-BT and PPF-SO-DHTBT polymers. Highly efficient B, G, and R PLEDs and low-threshold blue-green distributed feedback lasers are fabricated with these polymers and shown to possess impressive characteristics. In addition, highly efficient WPLEDs with high CRI and good color stability are realized for optimized B, G and R polymer blends.

## 2. Results and Discussion

### 2.1. Polymer Synthesis and Characterization

The synthetic routes to B, G and R light-emitting PPF-SO, PPF-SO-BT and PPF-SO-DHTBT are shown in **Scheme 1**. The SO (monomer M2), BT (M4) and DHTBT (M5) units were

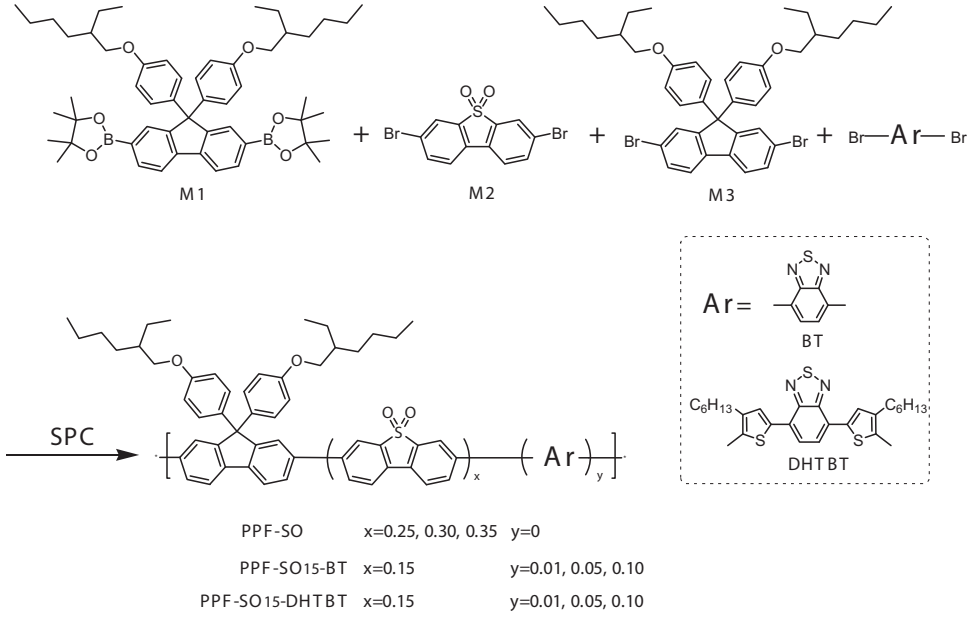


**Scheme 1.** Synthetic route for the PPF-SO, PPF-SO15-BT and PPF-SO15-DHTBT polymers.

**Table 1.** Selected properties of PPF-SO, PPF-SO15-BT and PPF-SO15-DHTBT polymers.

| Polymer | $M_n$ [×10$^4$] | PDI | $T_d$[a)] [°C] | $E_g$[b)] [eV] | HOMO [eV] | LUMO[c)] [eV] | $\Phi_{PL}$ [%] |
|---|---|---|---|---|---|---|---|
| PPF-SO25 | 6.85 | 1.64 | 434 | 2.83 | –5.96 | –3.13 | 53 |
| PPF-SO30 | 7.47 | 1.66 | 438 | 2.83 | –5.96 | –3.13 | 44 |
| PPF-SO35 | 5.42 | 2.08 | 438 | 2.82 | –5.96 | –3.14 | 51 |
| PPF-SO15-BT1 | 6.93 | 2.58 | 418 | 2.80 | –5.82 | –3.02 | 67 |
| PPF-SO15-BT5 | 6.15 | 2.44 | 423 | 2.45 | –5.80 | –3.35 | 56 |
| PPF-SO15-BT10 | 5.29 | 2.37 | 428 | 2.50 | –5.79 | –3.29 | – |
| PPF-SO15-DHTBT1 | 2.48 | 2.34 | 433 | 2.08 | –5.98 | –3.90 | 56 |
| PPF-SO15-DHTBT5 | 2.08 | 2.80 | 430 | 2.06 | –5.98 | –3.92 | 54 |
| PPF-SO15-DHTBT10 | 2.97 | 2.87 | 430 | 2.06 | –5.98 | –3.92 | 41 |

[a)]TGA determined thermal degradation temperature, corresponding to 5 wt% loss; [b)]Optical gap calculated from the absorption onset; [c)]LUMO energy estimated from the HOMO level and optical gap.

incorporated into a PPF (M1 and M3) backbone via Suzuki polycondensation (SPC). PPF and SO molar monomer feed ratios of 75:25, 70:30 and 65:35 were used to generate polymers PPF-SO25, PPF-SO30 and PPF-SO35. Polymers PPF-SO15-BT1, PPF-SO15-BT5 and PPF-SO15-BT10 were synthesized using PPF, SO and BT molar monomer feed ratios of 84:15:1, 80:15:5 and 75:15:10 and polymers PPF-SO15-DHTBT1, PPF-SO15-DHTBT5, PPF-SO15-DHTBT10 were synthesized using equivalent PPF, SO and DHTBT molar monomer feed ratios. All of these polymers are soluble in common organic solvents, such as toluene, chlorobenzene, chloroform, and tetrahydrofuran (THF). The polystyrene calibrated number-average molecular weight ($M_n$) and polydispersity index (PDI) was determined for each of the polymers by gel permeation chromatography (GPC) using THF as eluent; results are listed in **Table 1** and the chromatograms are shown in the Supporting Information Figure S1. $M_n$ values range from 54 200 to 74 700 with PDIs from 1.64 to 2.08 for the PPF-SO polymers, from 52 900 to 69 300 with PDIs from 2.37 to 2.58 for the PPF-SO-BT and from 20800 to 29700 with PDIs from 2.34 to 2.87 for the PPF-SO-DHTBT polymers. Polymer thermal stability was investigated by thermogravimetric analysis (TGA). The decomposition temperatures, $T_d$ (corresponding to 5 wt% loss) exceed 400 °C for all polymers (see Table 1).

### 2.2. Photophysical and Electrochemical Properties

The UV-Visible absorption spectra of polymer in toluene solution are shown in **Figure 1**a. The strong peak at ≈390 nm can be attributed to $\pi$–$\pi$* transitions of extended PPF-SO segments, while the additional absorptions peaked at ≈430 nm and 500 nm arise from the incorporation of BT and DHTBT units into the PPF chains, respectively.[14,22,23,40,41] Figure 1b shows the absorption spectra of the same polymers in thin film format. The absorption spectra for the films closely correspond to those in solution, other than for minor red-shifts and broadening of peaks and a more obvious long wavelength (≈515 nm)

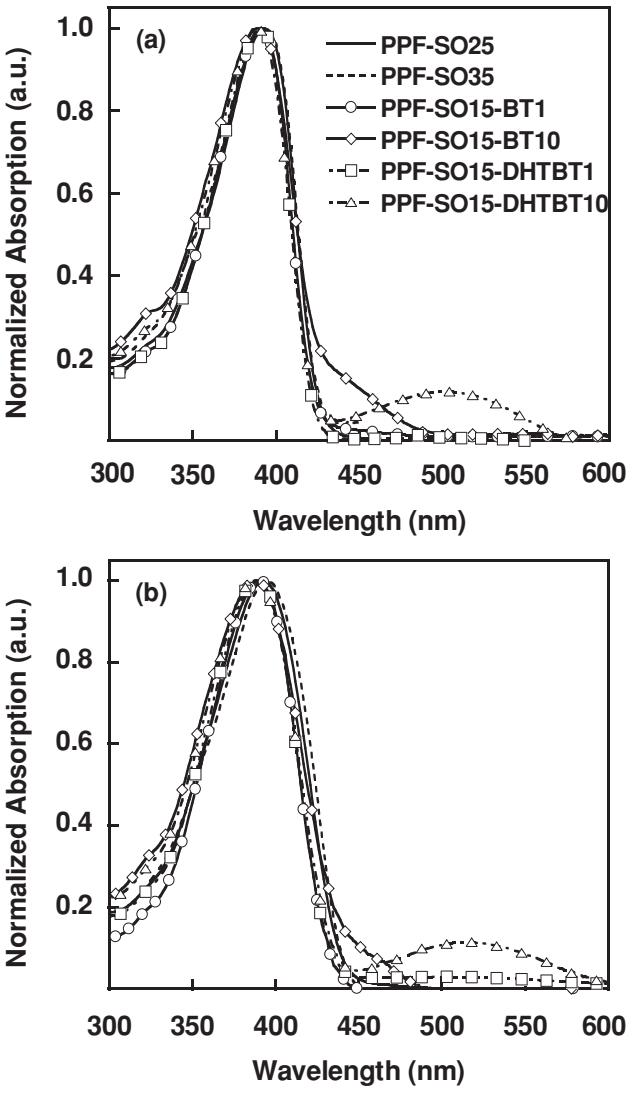


**Figure 1.** Peak normalized absorption spectra in a) toluene solution of $10^{-5}$ M and b) thin film of polymers PPF-SO25 (solid line), PPF-SO35 (dashed line), PPF-SO15-BT1 (solid line with circles), PPF-SO15-BT10 (solid line with diamonds), PPF-SO15-DHTBT1 (dashed line with squares) and PPF-SO15-DHTBT10 (dashed line with triangles).

absorption in PPF-SO15-DHTBT1. For example, the absorption peaks at ≈440 nm and 515 nm for PPF-SO15-BT10 and PPF-SO15-DHTBT10 are some 10 nm red-shifted in comparison to those in solution; such shifts can be ascribed to film packing effects that increase conjugation and the local dielectric constant.[42] A more detailed assessment of the spectral features shows that neither replacement of dialkyl with dialkoxy-phenyl substituents (PF to PPF) nor subsequent incorporation of SO units (PPF to PPF-SO) has much effect on the characteristic PF $\pi$–$\pi$* transition at ≈390 nm. Addition of 1% of BT or DHTBT also has little effect on absorption but 10% BT or DHTBT results in the appearance of a weak longer wavelength absorption feature and small changes on the short wavelength edge of the main PPF-SO peak. The 10% BT induced long wavelength peak at ≈440 nm is blue shifted relative to that (≈455 nm) in

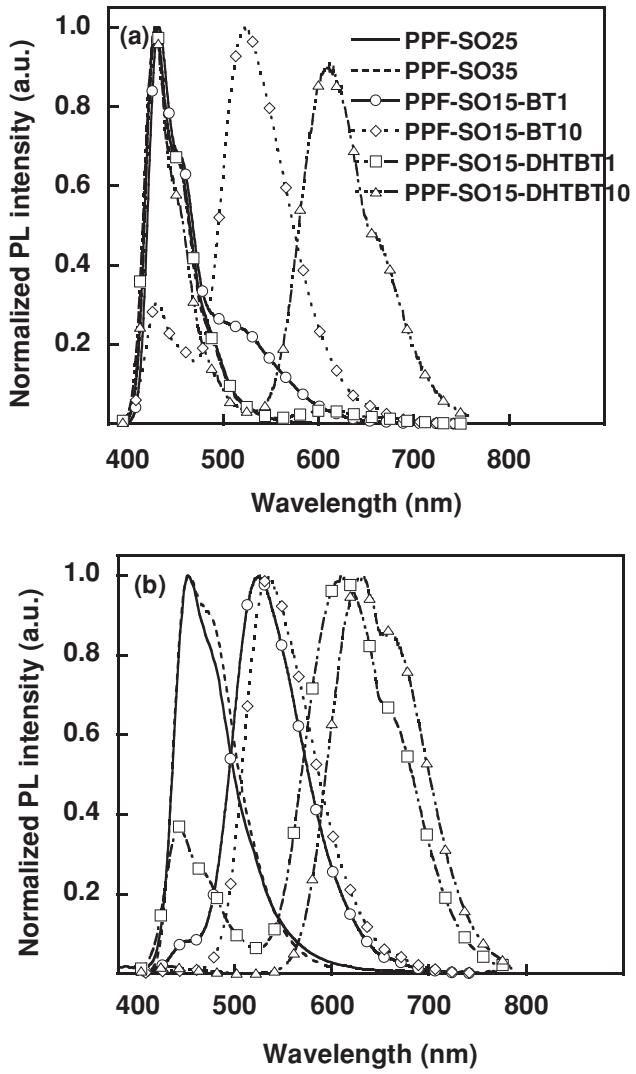


**Figure 2.** Peak normalized PL spectra in a) toluene solution of $10^{-5}$ M and b) thin film of polymers PPF-SO25 (solid line), PPF-SO35 (dashed line), PPF-SO15-BT1 (solid line with circles), PPF-SO15-BT10 (dashed line with diamonds), PPF-SO15-DHTBT1 (dashed line with squares) and PPF-SO15-DHTBT10 (dashed line with triangles).

the alternating copolymer of 9,9-dioctylfluorene (F8) and BT units (F8BT) but is at a similar position (≈440–445) to the peak in T4BT starburst compounds comprising a truxene core tri-substituted with quaterfluorene arms into each of which a single BT unit is inserted (giving an ≈16% BT unit fraction).[40] Hybridization of BT and PPF-SO molecular orbitals seems therefore to be incomplete; uninterrupted PPF-SO sequences act as distinct chromophores. A similar behavior is seen for the DHTBT units. Comparison of PPF-SO15-DHTBT10 with Dow Red F, comprising 50% F8, 40% BT, 5% TBT and 5% triarylamine units, shows that the long wavelength peak is blue-shifted; 515 nm versus 550 nm for Red F.[22,23,41]

The corresponding PL spectra are presented in **Figure 2**. In solution (Figure 2a), the PL is dominated by emission peaks at ≈430 nm (attributed to PPF-SO segments), ≈520 nm (attributed to BT containing segments) and ≈605 nm (attributed to DHTBT containing segments). Energy transfer via the Förster dipole-dipole mechanism is expected from PPF-SO segments to BT or DHTBT containing segments due to the spectral overlap of the PPF-SO emission with the BT and DHTBT absorptions.[43,44] This overlap is greater for the BT containing polymers (compare Figure 1a and 2a), consistent with a lower relative strength for the DHTBT PL emission components. However, even with incorporation of 10% BT there is still a residual PL in the blue indicating incomplete energy transfer from PPF-SO segments. The situation is even more obvious for the DHTBT polymers where there is an approximately equal contribution from blue and red emission components for 10% DHTBT. Figure 2b shows the PL spectra for the same polymers in thin film format. The PPF-SO polymers give PL peaked at ≈450 nm, red-shifted ≈20 nm from solution and somewhat broadened. The PPF-SO PL is also red-shifted relative to the thin film PL spectra for PFO and related 9,9-dialkylfluorene polymers[45] and other blue-light emission PFs such as F8DP[35,41,46,47] and BP156.[48] F8DP and BP156 have alternating 9,9-dioctylfluorene and, respectively, 9,9-dimethoxyphenylfluorene (F8DP) and 9,9-diphenylfluorene (BP156) units, indicating that it is the SO units that are responsible for this PL red shift rather than the 9,9-bis(4-(2-ethyl-hexyloxy)phenyl)fluorene units. The energy transfer from PPF-SO to BT/DHTBT-containing segments is significantly enhanced in the solid state relative to solution, likely to be the result of enhanced exciton migration through inter-molecular interactions.[25,49] Again, transfer to BT-containing segments occurs more readily, as demonstrated by the larger residual blue emission component for PPF-SO15-DHTBT1 films than for PPF-SO15-BT1 films. A 10% fraction of BT/DHTBT units in thin film samples is, however, more or less sufficient to wholly quench the PPF-SO blue emission component. Increasing fractions of BT/DHTBT lead to a red-shift in the longest wavelength emission component; for example, in the case of PPF-SO15-DHTBT1, the emission peaks at ≈610 nm, whilst for PPF-SO15-DHTBT10 it peaks at ≈630 nm. Similar behavior is observed for the PPF-SO15-BT polymers. Related behavior was also seen for Red F (containing 5% TBT units) where dispersion in a blend with F8BT led to a significant blue shift in amplified spontaneous emission (ASE) wavelength.[41]

The polymer thin film PL quantum efficiency ($\Phi_{PL}$) values were measured with an integrating sphere as described below. The, respectively, R, G and B light-emitting PPF-SO-DHTBT, PPF-SO-BT and PPF-SO polymers all have $\Phi_{PL}$ >40% (see Table 1). $\Phi_{PL}$ decreases from 67% for PPF-SO15-BT1 to 56% for PPF-SO15-BT5 and from 56% for PPF-SO15-DHTBT1 to 41% for PPF-SO15-DHTBT10. This suggests an unfavourable PL quenching with increasing BT/DHTBT fraction, quite possibly as a result of greater interchain interactions; again similar behavior is seen for Red F:F8BT and poly(3-hexylthiophene) (P3HT):F8BT blends where $\Phi_{PL}$ values increase with increasing dilution.[41,50] Further studies will be required to more fully understand the changes in $\Phi_{PL}$.

The electrochemical properties of the polymers were investigated by cyclic voltammetry (CV), with ferrocene as internal standard. The highest occupied molecular orbital (HOMO) energies were estimated according to the empirical formula $E_{HOMO} = -e(E_{ox} + 4.80)$ eV.[51] The lowest unoccupied molecular

orbital (LUMO) energies were then deduced from the HOMO energies by subtraction of the corresponding optical gap energy; a procedure that is not expected to be highly accurate but which should suffice to follow trends. As shown in Table 1, the HOMO level energies of the PPF-SO, PPF-SO15-BT and PPF-SO15-DHTBT polymers are estimated to be −5.96, −5.80 and −5.98 eV (relative to vacuum), respectively. The corresponding LUMO levels are then −3.13, −3.30 and −3.90 eV. It is evident that the LUMO levels decrease with incorporation of BT and DHTBT units, as also seen for F8BT relative to PFO.

### 2.3. Electroluminescence Characteristics of Red, Green and Blue PLEDs

LEDs were fabricated with a device configuration comprising ITO/PEDOT:PSS/emission polymer/CsF/Al. Electroluminescence (EL) spectra recorded at 10 mA $cm^{-2}$ current density are shown in **Figure 3**, with peaks at ≈450, ≈530 and ≈620 nm, respectively, for PPF-SO, PPF-SO15-BT1 and PPF-SO15-DHTBT1 emission polymers. The EL spectra of the green and red light-emitting polymers red-shift with increasing fractions of BT and DHTBT units; PPF-SO15-BT10 LEDs emit at 545 nm while PPF-SO15-DHTBT10 LEDs emit at 650 nm.

EL spectral stability is an important concern for blue light-emitting polymers and we note that the spectra for PPF-SO30 LEDs are almost unchanged on annealing for 2 h at a sequence of temperatures between 80 and 200 °C and also for current densities from 5 to 105 mA $cm^{-2}$ (see Supporting Information Figure S2). This is considered to be a consequence of both the bulky alkoxyphenyl substituent at the C-9 position of the PPF unit and the electron-withdrawing SO unit mitigating against fluorenone formation.[16d]

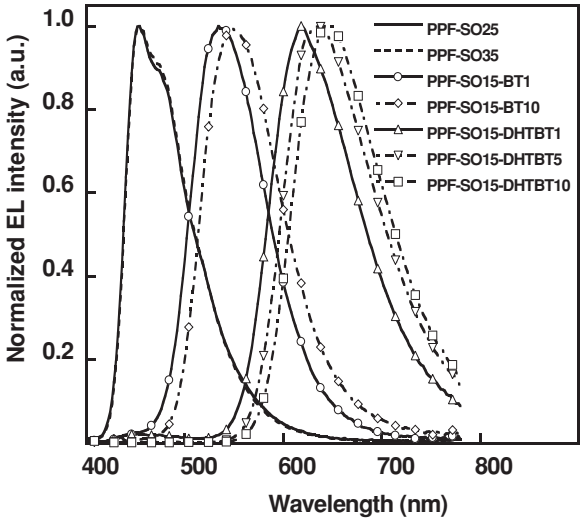


**Figure 3.** EL spectra of PLEDs using emission polymers PPF-SO25 (solid line), PPF-SO35 (dashed line), PPF-SO15-BT1 (solid line with circles), PPF-SO15-BT10 (dashed line with diamonds), PPF-SO15-DHTBT1 (solid line with up triangles), PPF-SO15-DHTBT5 (dashed line with down triangles) and PPF-SO15-DHTBT10 (dashed line with squares) with the configuration of ITO/PEDOT:PSS/emission polymer/CsF/Al.

More detailed PLED characteristics are summarized in **Table 2**. For the ITO/PEDOT:PSS/emission polymer/CsF/Al devices, best B, G and R LED performances were obtained with PPF-SO25, PPF-SO15-BT1, and PPF-SO15-DHTBT1, respectively. Turn on voltages, $V_{on}$ = 3.2, 3.2 and 4.9 V and efficiencies $LE_{max}$ = 4.3, 14.9 and 2.8 cd $A^{-1}$, respectively, were achieved. Insertion of a poly(N-vinyl-carbazole) (PVK) film as a hole injection layer atop the PEDOT:PSS improves device performance further with $LE_{max}$ = 7.0, 17.6 and 4.3 cd $A^{-1}$ obtained for PPF-SO25, PPF-SO15-BT1, and PPF-SO15-DHTBT1, respectively, with corresponding CIE coordinates B = (0.15, 0.17), G = (0.37, 0.56) and R = (0.62, 0.36). Balanced charge injection and transport are expected to play a significant role in the improvement.[16d]

Performance of the red LEDs was further enhanced by insertion of a hole-blocking/electron-transporting TPBI layer beneath the cathode. This was expected to help better confine excitons within the emission layer[52] and, indeed, resulted in a dramatic improvement in performance, with $LE_{max}$ = 6.1 cd $A^{-1}$ achieved for PPF-SO15-DHTBT1. To the best of our knowledge, this is the highest efficiency reported to date for a fluorescent red light-emitting fluorene-based PLED.

The luminance efficiency and luminance versus current density (LE and $L$ vs $J$) characteristics of B, G and R PLEDs are shown in **Figure 4**. At a current density of 100 mA $cm^{-2}$, the LE values for PPF-SO25, PPF-SO15-BT1 and PPF-SO15-DHTBT1 based LEDs are 6.3, 12.0 and 3.5 cd $A^{-1}$, respectively. We note that the LE values decline rather slowly with increasing current density, suggesting relatively good stability for these PLEDs.

### 2.4. Amplified Spontaneous Emission (ASE) and Laser Emission

Thermally and morphologically stable conjugated polymers have been shown to be promising active materials for low-cost organic solid-state lasers.[41,45,47,53–57] Here we focus on the optical gain properties of the blue light-emitting PPF-SO polymers which, as shown above, have high $\Phi_{PL}$ values and excellent spectral stability. **Figure 5** shows representative PL, ASE and laser emission spectra for PPF-SO35 films on silica substrates (PL and ASE, 130 nm and 145 nm film thicknesses, respectively) and on surface grating patterned (grating period $\Lambda$ = 290 nm, fill factor 50%, etch depth 90 nm) fused silica substrates (laser emission at 476 nm at 140 nm film thickness). The low pump pulse energy PL spectrum changes drastically as the pump pulse energy is increased. A sharp ASE peak emerges at the 475 nm 0–1 vibronic, corresponding to a favourable four-level gain process[41] and eventually grows to dominate the spectrum. In order to facilitate comparison with the literature, we define the pump pulse energy at which the full width at half maximum (FWHM) linewidth of the spectrum drops to half its (low pump pulse energy) PL value as the threshold energy, $E_{th}$.[47] An alternative threshold energy measure comes from the observation of a kink in the output versus input intensity ($I_{out}$ vs $I_{in}$) characteristics (see Supporting Information Figure S3). $E_{th}$ values of 0.39, 0.25 and 0.25 μJ were estimated, respectively, for PPF-SO25, PPF-SO30 and PPF-SO35 polymers. These compare with $E_{th}$ values of 0.32, 0.1 and 0.1 μJ for polymers PFO, F8DP and BP156,[41,48] respectively, suggesting PPF-SO

**Table 2.** Device performance parameters for PPF-SO (Blue), PPF-SO15-BT (Green) and PPF-SO15-DHTBT (Red) PLEDs.

| Polymer | $V_{on}$[a)] [V] | $L_{max}$ [cd m$^{-2}$] | $LE_{max}$ [cd A$^{-1}$] | $V$ [V] | $L$ [cd m$^{-2}$] | LE [cd A$^{-1}$] | CIE[b)] [x, y] |
|---|---|---|---|---|---|---|---|
| PPF-SO25 | 3.2[c)] | 8577 | 4.3 | 5.0 | 3984 | 4.1 | (0.16, 0.19) |
| | 3.0[d)] | 12080 | 7.0 | 5.8 | 6346 | 6.3 | (0.15, 0.17) |
| PPF-SO30 | 5.4[c)] | 4235 | 2.4 | 8.7 | 2264 | 2.4 | (0.17, 0.19) |
| | 3.3[d)] | 10883 | 6.6 | 6.9 | 5769 | 5.8 | (0.16, 0.22) |
| PPF-SO35 | 4.3[c)] | 4910 | 2.5 | 6.5 | 2412 | 2.5 | (0.17, 0.20) |
| | 3.6[d)] | 6776 | 4.7 | 8.2 | 4265 | 3.9 | (0.16, 0.22) |
| PPF-SO15-BT1 | 3.2[c)] | 31225 | 14.9 | 4.4 | 313 | 13.7 | (0.35, 0.58) |
| | 5.7[d)] | 30314 | 17.6 | 11.7 | 12120 | 12.0 | (0.37, 0.56) |
| PPF-SO15-BT5 | 3.3[c)] | 15418 | 7.1 | 6.3 | 4856 | 4.9 | (0.41, 0.57) |
| | 4.8[d)] | 22670 | 13.9 | 10.2 | 10179 | 9.1 | (0.41, 0.56) |
| PPF-SO15-BT10 | 5.0[c)] | 4747 | 1.7 | 8.3 | 1909 | 1.6 | (0.41, 0.56) |
| | 7.7[d)] | 6536 | 6.9 | 20.8 | 2225 | 2.4 | (0.43, 0.55) |
| PPF-SO15-DHTBT1 | 4.9[c)] | 5047 | 2.8 | 8.2 | 1669 | 1.6 | (0.61, 0.37) |
| | 7.7[d)] | 9855 | 4.3 | 13.3 | 2943 | 2.5 | (0.62, 0.36) |
| | 5.4[e)] | 6957 | 6.1 | 10.8 | 2936 | 3.5 | (0.62, 0.36) |
| PPF-SO15-DHTBT5 | 4.7[c)] | 1892 | 1.8 | 9.1 | 1092 | 1.0 | (0.65, 0.34) |
| | 7.4[d)] | 3321 | 2.5 | 14.4 | 1624 | 1.4 | (0.66, 0.34) |
| | 4.8[e)] | 2790 | 3.5 | 12.3 | 1806 | 1.8 | (0.66, 0.34) |
| PPF-SO15-DHTBT10 | 4.4[c)] | 2351 | 1.5 | 8.0 | 1096 | 1.1 | (0.66, 0.33) |
| | 5.3[d)] | 4479 | 3.3 | 11.7 | 1608 | 1.8 | (0.67, 0.33) |
| | 4.5[e)] | 4369 | 4.3 | 11.7 | 2509 | 2.7 | (0.67, 0.32) |

[a)] $V_{on}$ is defined as the voltage at which a luminance of 1 cd m$^{-2}$ is reached. $L_{max}$ and $LE_{max}$ are the maxima luminance (cd m$^{-2}$) and luminous efficiency (cd A$^{-1}$) values recorded for each device. $V$, $L$, LE are the voltage, luminance and luminous efficiency values recorded at a current density $J$ = 100 mA cm$^{-2}$; [b)]CIE color coordinates are measured at J = 10 mA cm$^{-2}$. [c)] Device structure: ITO/PEDOT:PSS/emission polymer/CsF/Al; [d)]Device structure: ITO/PEDOT:PSS/PVK/emission polymer/CsF/Al; [e)]Device structure: ITO/PEDOT:PSS/emission polymer/TPBI/CsF/Al.

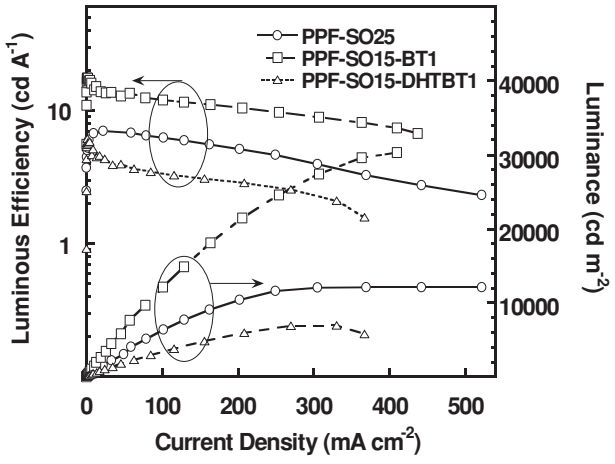


**Figure 4.** Device characteristics (LE (cd A$^{-1}$) and $L$ (cd m$^{-2}$) versus $J$ (mA cm$^{-2}$)) for PLEDs based on PPF-SO25 (solid line with circles), PPF-SO15-BT1 (dashed line with squares) and PPF-SO15-DHTBT1 (dashed line with triangles) polymer emission layers.

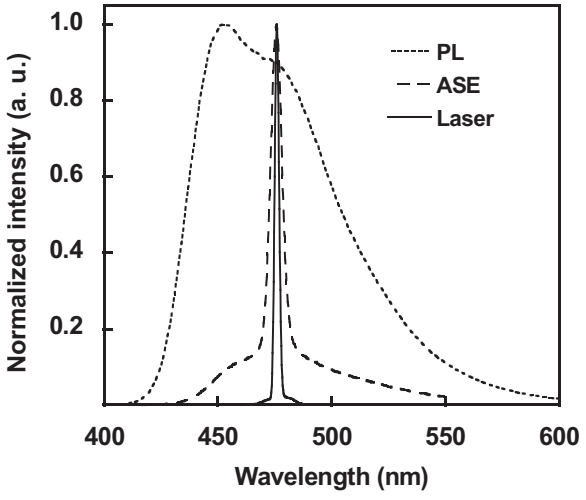


**Figure 5.** PL (dotted line) and ASE (dashed line) spectra for PPF-SO35 films of 130 and 145 nm thickness, respectively, spin-coated on quartz substrates. The laser emission (solid line) spectrum for a 140 nm thickness film spin coated on top of a grating-patterned (290 nm period, 50% fill factor, 90 nm etch depth) spectrosil substrated is also shown.

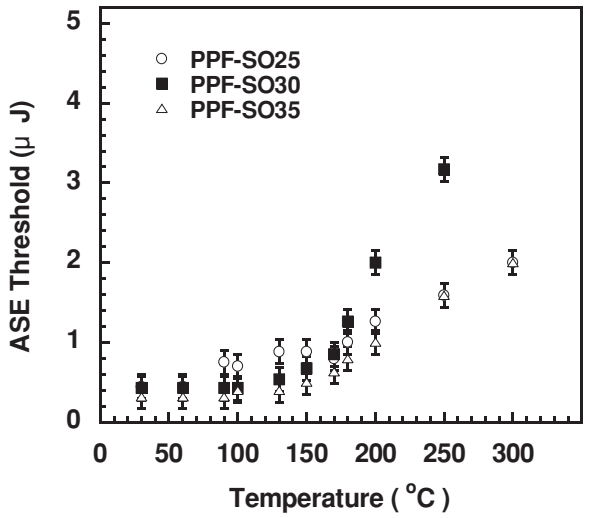


**Figure 6.** ASE threshold energies plotted as a function of annealing temperature for polymers PPF-SO25, PPF-SO30 and PPF-SO35.

polymers are attractive gain media for use in solid-state polymer lasers and amplifiers.

The thermal stability of the gain properties was assessed by measuring the ASE characteristics following annealing at different temperatures. The PPF-SO polymer films were annealed in a $N_2$-filled glove box for 10 min at a sequence of temperatures between 30 and 300 °C with ASE measurements performed externally to the box after each annealing step. **Figure 6** shows the corresponding variation in ASE threshold. PPF-SO35, in particular, displays an excellent ASE threshold stability; there is little change in $E_{th}$ up to ≈130 °C. Beyond this temperature, ASE could still be observed but there is a gradual increase in threshold, rising some five-fold between 130 and 300 °C. In comparison, the ASE threshold measured under similar condition for PFO has been reported to increase from 0.32 to 2.0 μJ pulse$^{-1}$ on annealing from room temperature to 130 °C, with ASE no longer apparent once the annealing temperature reached 150 °C.[47] The raised ASE threshold stability of PPF-SO35 compared with PFO is in part due to an absence of crystallization and thereby reduced optical scattering losses,[54,55] being consistent with high glass transition temperature $T_g$ = 223 °C and no distinct melting process below 300 °C (see Supporting Information Figure S4). High thermal stability is also seen for F8DP and for poly(9-spiro(10,10-*bis*(2-ethylhexyl)-10*H*-anthracene)fluorene) (PEHSAF) for which the ASE thresholds were largely unaltered up to 230 °C (where F8DP melts) and 250 °C (the experimental limit of the apparatus), respectively.[47] Neither F8DP nor PEHSAF appear to crystallize; PEHSAF shows no thermal transition features in digital scanning calorimetry measurements before the onset of degradative weight loss (observed in thermal gravimetric analysis at 367 °C).[47] PPF-SO35 is not, therefore, as stable as F8DP or PEHSAF but performs well relative to PFO.

Distributed feedback (DFB) lasers were also fabricated and the laser emission wavelength was tuned by varying the polymer film thickness spin-coated on the grating-patterned fused silica substrates. For a grating with period $\Lambda$ = 290 nm, fill factor 50% and etch depth 90 nm, varying the polymer thickness from 110 to 152 nm gave laser emission across the range 467 to 487 nm (see Supporting Information Figure S5). The lowest lasing threshold of 18.0 nJ per pulse was achieved for a laser operating at 485 nm using a 134 nm thickness PPF-SO30 film.

### 2.5. White Light Emission PLEDs Based on Polymer Blends

PLEDs with PPF-SO25 (B), PPF-SO15-BT1 (G) and PPF-SO15-DHTBT1 (R) emission layers give EL spectra that cover the entire visible spectrum (see Figure 3). We can expect, therefore, that blends of these materials will allow white light PLEDs (WPLEDs) to be fabricated with spectral properties that can be tuned by careful control of blend ratio. Type I devices with the configuration of ITO/PEDOT:PSS/B:G:R polymer blend/CsF/Al were fabricated using different B, G and R polymer fractions. The resulting EL spectra show components peaked at 455, 535 and 620 nm (see Supporting Information Figure S6) corresponding to emission from PPF-SO25, PPF-SO15-BT1 and PPF-SO15-DHTBT1, respectively. Optimization of the B:G:R blend composition to a ratio 100:8:7 by weight yields a well-balanced white emission with CIE coordinates (0.33, 0.36) and device efficiencies $LE_{max}$ = 6.7 cd A$^{-1}$ and $PE_{max}$ = 5.5 lm W$^{-1}$ (c.f. **Table 3** for a comparison of data for different blend

**Table 3.** Device performance parameters for WPLEDs.

| Device Type[a)] | B:G:R[b)] [wt:wt] | $LE_{max}$ [cd A$^{-1}$] | $PE_{max}$ [lm W$^{-1}$] | $L_{max}$ [cd m$^{-2}$] | LE [cd A$^{-1}$] | PE [lm W$^{-1}$] | CIE[c)] [x, y] | CCT[c)] [K] | CRI[c)] |
|---|---|---|---|---|---|---|---|---|---|
| I | 100:8:5 | 7.1 | 6.5 | 9493 | 6.5 | 4.5 | (0.29, 0.35) | 7243 | 84 |
| II | 100:8:5 | 9.0 | 8.1 | 9881 | 8.0 | 5.0 | (0.33, 0.37) | 5605 | 89 |
| I | 100:8:7 | 6.7 | 5.5 | 9658 | 6.2 | 3.9 | (0.33, 0.36) | 5696 | 90 |
| II | 100:8:7 | 9.8 | 8.9 | 10079 | 8.5 | 5.6 | (0.36, 0.37) | 4632 | 91 |
| I | 100:8:9 | 6.1 | 5.1 | 8992 | 5.5 | 3.5 | (0.34, 0.36) | 5111 | 91 |
| II | 100:8:9 | 8.5 | 7.4 | 8988 | 7.6 | 5.0 | (0.38, 0.37) | 3974 | 91 |

[a)]Device Type I: ITO/PEDOT:PSS/B:G:R polymer blend/CsF/Al; Device Type II: ITO/PEDOT:PSS/B:G:R polymer blend/PFN/CsF/Al; [b)]B:G:R polymers are PPF-SO25, PPF-SO15-BT1 and PPF-SO15-DHTBT1, respectively. $LE_{max}$, $PE_{max}$ and $L_{max}$ are the maxima luminous efficiency (cd A$^{-1}$), power efficiency (lm W$^{-1}$) and luminance (cd m$^{-2}$) values recorded for each device. LE and PE are the luminous and power efficiencies recorded at 3000 cd m$^{-2}$; [c)]WPLED color coordinates (CIE), color temperature (CCT) and color rendering index (CRI) are measured at $J$ = 10 mA cm$^{-2}$.

compositions). The excess B component is required to compensate for the energy transfer from B to both G and R polymers that follows generation of an exciton within the B polymer. In principle, transfer from G to R polymers is also possible but their degree of dilution within the B polymer matrix makes this substantially less probable. Interestingly, white light emission blends of F8DP (B), F8BT (G) and Red F (R) polymers used as down conversion media for 370 nm AlInGaN LEDs are optimized at a lower G and R fraction, namely B: G: R = 99.0:0.6:0.4 wt%, emphasising the complexity of the differences in exciton formation and decay under optical and electrical pumping conditions.[35]

In Type II WPLEDs a 20-nm thickness poly[(9,9-bis(3′-(*N*,*N*-dimethylamino)propyl)-2,7-fluorene)-*alt*-2,7-(9,9-dioctylfluorene)] (PFN) electron-injection layer (EIL)[58,59] was inserted between the light-emitting polymer blend and the cathode to give a device configuration ITO/PEDOT:PSS/B:G:R polymer blend/PFN/CsF/Al. This greatly improved WPLED performance through more efficient electron injection and better-balanced carrier transport. Then, as reported in Table 3, we were able to achieve $LE_{max}$ = 9.8 cd $A^{-1}$ (at 3.7 mA $cm^{-2}$ current density) and $PE_{max}$ = 8.9 lm $W^{-1}$ (at 0.4 mA $cm^{-2}$ current density). In addition, the CIE coordinates (0.36, 0.37) were found to remain very close to the ideal white point (0.33, 0.33). The relative intensity of R emission increased when the PFN EIL was introduced (see Supporting Information Figure S6) leading to a spectrum for 100:8:7 blend WPLEDs containing a PFN EIL that closely resembles that of the 100:8:9 blend without the EIL. This strongly suggests that electron injection and trapping on the PPF-SO15-DHTBT1 red light-emitting polymer are enhanced by use of the EIL.[60]

**Figure 7**a displays the current density and luminance versus voltage (*J*/*L* vs*V*) characteristics and Figure 7b the luminous and power efficiency versus current density (LE/PE vs*J*) characteristics for 100:8:7 blend WPLEDs both with (dashed line, half-filled squares) and without (solid line, empty circles) a PFN EIL. The sharp luminance turn-on at $V_{on} \approx 3.0$ V helps to achieve high power efficiency at relatively high luminance levels. For example, we find $LE_{max}$ = 8.5 cd $A^{-1}$ and $PE_{max}$ = 5.6 lm $W^{-1}$ for a forward-emitted luminance of 3000 cd $m^{-2}$; to the best of our knowledge, this is one of the best performances reported in the literature for all-fluorescent WPLEDs.

For lighting applications, the color quality must also be considered. Relatively high CRI values (89–91) are achieved for all of the devices listed in Table 3 with the exception of the Type I device with blend ratio 100:8:5 for which the CRI is only 84. Corresponding color temperatures fall in the range 3974–5696 K with again the Type I device with blend ratio 100:8:5 an outlier with color temperature 7243 K. The key feature of this device's EL spectrum is its relatively weak R emission component, something that as already noted above, is improved by an increase of the R polymer fraction in the blend and/or insertion of a PFN EIL. The full width at half-maximum linewidths for all of these devices are ≈230 nm.

The Type II device with blend ratio 100:8:7 has CRI = 91 and color temperature = 4630 K, very close to the 4700 K color temperature of sunlight at solar altitude 20°.[61] **Figure 8** displays the EL spectra for this device at a range of current densities. The corresponding CIE coordinates shift from (0.35, 0.37) to (0.33, 0.36) as the current density increases from 20 to 260 mA $cm^{-2}$ i.e., the CIE coordinate variations are limited to $\Delta_{x,y} \leq 0.02, 0.01$. The CRI also remains essentially more than 90.

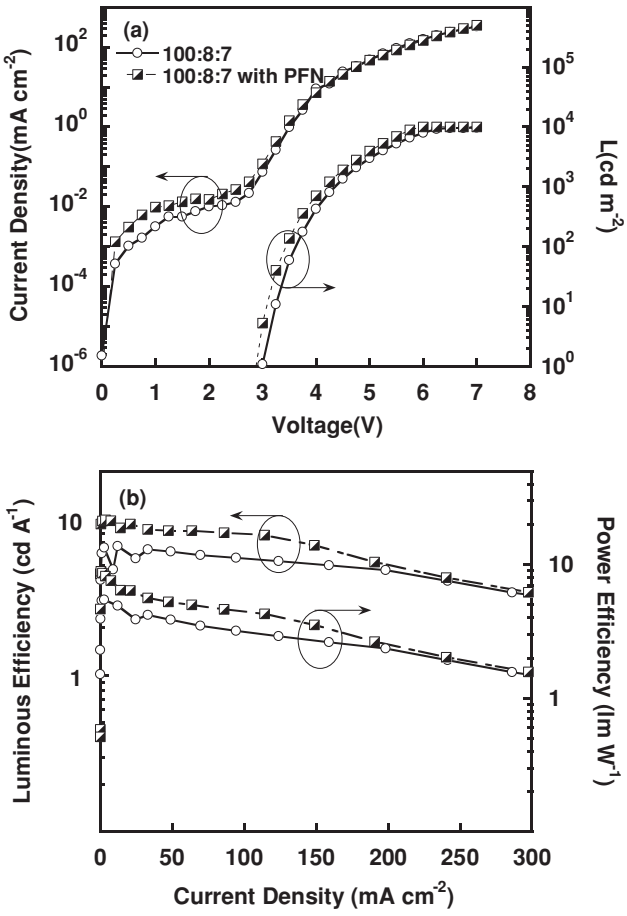


**Figure 7.** a) Current density and luminance versus voltage (*J*/*L* vs *V*) and b) luminous and power efficiency versus current density (LE/PE vs *J*) characteristics for 100:8:7 blend WPLEDs both with (dashed line, half-filled squares) and without (solid line, empty circles) a PFN electron injection layer.

The excellent current density invariance observed for these devices is attributed to the fact that the PPF-SO15 (B), PPF-SO15-BT1 (G) and PPF-SO15-DHTBT1 (R) light-emitting polymers have very similar chemical structures and show no evidence for crystallization, helping to limit the tendency to phase separate and thereby enhancing stability. Atomic force microscopy (AFM) was used to further investigate the phase morphology of the blend system. The AFM phase images (see Supporting Information Figure S7) of both the pure polymer and the blend film are very similar, which clearly indicate no significant phase separation occurred; the root-mean-square(RMS) surface roughnesses recorded for a polymer PPF-SO25 and for blend film are respectively 0.68 nm and 0.67 nm, which imply a better compatibility in the blend components.[62–64]

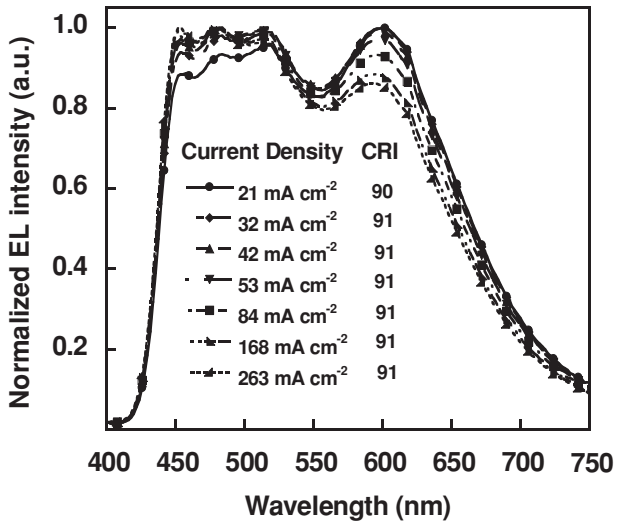


**Figure 8.** EL spectra measured for an ITO/PEDOT:PSS/100:8:7 emission polymer blend/PFN/CsF/Al WPLED at 20 (filled circles), 32 (filled diamonds), 42 (filled up triangles), 53 (filled down triangles), 84 (filled squares), 168 (filled left triangles), 263 (filled right triangles) mA $cm^{-2}$ current densities.

## 3. Summary and Conclusions

In summary, we have reported the synthesis, characterization and application of a series of blue (B), green (G) and red (R) light-emitting PPF-SO, PPF-SO-BT and PPF-SO-DHTBT polymers. All of these polymers exhibit high PL yields (>40%) and have good thermal stability (decomposition temperature > 400 °C). PLEDs using PPF-SO25, PPF-SO15-BT1 and PPF-SO15-DHTBT1 give maximum efficiencies $LE_{max}$ = 7.0, 17.6 and 4.3 cd $A^{-1}$ with CIE coordinates (0.15, 0.17), (0.37, 0.56) and (0.62, 0.36), respectively. $LE_{max}$ was increased to 6.1 cd $A^{-1}$ for PPF-SO15-DHTBT1 by inserting a hole-blocking/electron-transporting TPBI layer. In addition, 1D distributed feedback lasers using PPF-SO30 as gain medium were demonstrated, with a wavelength tuning range 467 – 487 nm and low pump energy thresholds (≥18 nJ). Blending different ratios of PPF-SO, PPF-SO-BT and PPF-SO-DHTBT polymers allows highly efficient WPLEDs to be realized. With a diode configuration incorporating a PFN EIL and a B:G:R blend ratio 100:8:7 by weight, $LE_{max}$ reaches 9.8 cd $A^{-1}$ and the maximum power efficiency, $PE_{max}$ reaches 8.9 lm $W^{-1}$. This is one of the best performance levels among all-fluorescent WPLEDs. Moreover, the optimized devices can have an attractive color temperature close to 4700 K and an excellent CRI ≥ 90. They are also relatively stable, with the emission color remaining almost unchanged as the current density increases from 20 to 260 mA $cm^{-2}$; the CIE coordinate shifts are limited to $\Delta_{x,y} \leq 0.02, 0.01$. These newly synthesized PPF-SO, PPF-SO-BT and PPF-SO-DHTBT polymers enable WPLEDs with a superior trade-off between device efficiency, CRI and color stability.

## 4. Experimental Section

*Materials and Characterization*: Reagents were distilled from appropriate drying agents prior to use. Commercially available reagents were used without further purification. 2,7-Bis(4′,4′,5′,5′-tetramethyl-1′,3′,2′-dioxaboralan-2′-yl)-9,9-bis(4-(2ethylhexyoxy) phenyl) fluorene(M1),[16d] 3,7-dibromo-dibenzothiophene-*S*,*S*-dioxide (M2),[16d] 2,7-dibromo-9,9-bis-(4-(2-ethylhexyloxy)phenyl)fluorene (M3),[16d] 4,7-dibromo-2,1,3-benzothiadiazole (M4)[19] and 4,7-bis(5-bromo-4-hexyl-2-thienyl)-2,1,3-benzothiadiazole (M5)[25] were prepared according to the literature. The general procedures used for Suzuki polycondensation (SPC), taking PPF-SO25 as an example are as follows: A mixture of monomer M1 (413 mg, 0.5 mmol), M2 (93.5 mg, 0.25 mmol), and M3 (183 mg, 0.25 mmol), $Pd(acetate)_2$ (1.5 mg), and tricyclohexylphosphine (3 mg) was dissolved in a mixture of toluene (4 mL) and THF (4mL) under an argon atmosphere. The mixture was heated to 90 °C and stirred, then $(Et)_4NOH$ (2 mL) and deionized water (2 mL) were added into the mixture. The solution was kept in the region of 90–100 °C with vigorous stirring under argon for 48 h. The end groups were capped by refluxing for 6 h with M1 and then bromobenzene. After cooling, the resulting polymer was precipitated into 100 mL of methanol, re-dissolved in dichloromethane, and then washed three times with water. A second precipitatation in methanol followed by washing with acetone (to remove oligomers and catalyst residues) and drying in vacuo yielded the product.

PPF-SO25:$^1$H NMR (300 MHz, $CDCl_3$) δ (ppm): 8.02 (s, ArH), 7.82 (br, ArH), 7.66-7.56 (br, ArH), 7.18 (br, ArH), 6.78 (br, ArH), 3.78 (br, O-$CH_2$), 1.68 (br, $CH_2$), 1.42-1.30 (br, $CH_2$), 0.89–0.87 (br, $CH_3$). Anal. Calcd (%) for $[(C_{41}H_{48}O_2)_{75}(C_{12}H_6O_2S)_{25}]_n$: C 83.90; H 7.82; S 1.66. Found: C 83.47; H 8.03; S 1.80.

PPF-SO30:$^1$H NMR (300 MHz, $CDCl_3$) δ (ppm): 8.03 (s, ArH), 7.91-7.82 (br, ArH), 7.66-7.55 (br, ArH), 7.21-7.17 (br, ArH), 6.84-6.75 (br, ArH), 3.80-3.78 (br, O-$CH_2$), 1.67 (br, $CH_2$), 1.44-1.22 (br, $CH_2$), 0.91–0.89 (br, $CH_3$). Anal. Calcd (%) for $[(C_{41}H_{48}O_2)_{70}(C_{12}H_6O_2S)_{30}]_n$: C 83.39; H 7.67; S 2.07. Found: C 83.09; H 7.95; S 1.92.

PPF-SO35:$^1$H NMR (300 MHz, $CDCl_3$) δ (ppm): 8.03 (s, ArH), 7.90-7.82 (br, ArH), 7.66-7.57 (br, ArH), 7.22-7.17 (br, ArH), 6.91-6.75 (br, ArH), 3.80-3.79 (br, O-$CH_2$), 1.68 (br, $CH_2$), 1.45-1.26 (br, $CH_2$), 0.92–0.87 (br, $CH_3$). Anal. Calcd (%) for $[(C_{41}H_{48}O_2)_{65}(C_{12}H_6O_2S)_{35}]_n$: C 82.83; H 7.50; S 2.51. Found: C 82.69; H 7.91; S 2.29.

PPF-SO15-BT1:$^1$H NMR (300 MHz, $CDCl_3$) δ (ppm): 8.02 (s, ArH), 7.81-7.74 (br, ArH), 7.66-7.56 (br, ArH), 7.21-7.15 (br, ArH), 6.81-6.75 (br, ArH), 3.78 (br, O-$CH_2$), 1.68 (br, $CH_2$), 1.50-1.30 (br, $CH_2$), 0.96–0.87 (br, $CH_3$). Anal. Calcd (%) for $[(C_{41}H_{48}O_2)_{84}(C_{12}H_6O_2S)_{15}(C_6H_2N_2S)_1]_n$: C 84.72; H 8.08; N < 0.3%; S 1.00. Found: C 84.63; H 8.41; N < 0.3; S 1.04.

PPF-SO15-BT5:$^1$H NMR (300 MHz, $CDCl_3$) δ (ppm): 8.04 (s, ArH), 7.79-7.73 (br, ArH), 7.66-7.55 (br, ArH), 7.24-7.09 (br, ArH), 6.81-6.75 (br, ArH), 3.78 (br, O-$CH_2$), 1.68 (br, $CH_2$), 1.50-1.30 (br, $CH_2$), 0.91–0.87 (br, $CH_3$). Anal. Calcd (%) for $[(C_{41}H_{48}O_2)_{80}(C_{12}H_6O_2S)_{15}(C_6H_2N_2S)_5]_n$: C 84.32; H 7.99; N < 0.3; S 1.29. Found: C 84.22; H 7.86; N < 0.3; S 1.38.

PPF-SO15-BT10:$^1$H NMR (300 MHz, $CDCl_3$) δ (ppm): 8.02 (s, ArH), 7.81-7.74 (br, ArH), 7.66-7.55 (br, ArH), 7.22-7.16 (br, ArH), 6.78 (br, ArH), 3.78 (br, O-$CH_2$), 1.68 (br, $CH_2$), 1.47-1.30 (br, $CH_2$), 0.91–0.87 (br, $CH_3$). Anal. Calcd (%) for $[(C_{41}H_{48}O_2)_{75}(C_{12}H_6O_2S)_{15}(C_6H_2N_2S)_{10}]_n$: C 83.79; H 7.87; N 0.59; S 1.69. Found: C 83.77; H 7.90; N 0.59; S 1.97.

PPF-SO15-DHTBT1:$^1$H NMR (300 MHz, $CDCl_3$) δ (ppm): 8.02 (s, ArH), 7.82-7.74 (br, ArH), 7.63-7.56 (br, ArH), 7.18-7.16 (br, ArH), 6.81-6.75 (br, ArH), 3.79-3.77 (br, O-$CH_2$), 1.68 (br, $CH_2$), 1.50-1.26 (br, $CH_2$), 0.91–0.89 (br, $CH_3$). Anal. Calcd (%) for $[(C_{41}H_{48}O_2)_{84}(C_{12}H_6O_2S)_{15}(C_{26}H_{30}N_2S_3)_1]_n$: C 84.64; H 8.08; N < 0.3; S 1.11. Found: C 84.52; H 8.24; N < 0.3; S 1.47.

PPF-SO15-DHTBT5:$^1$H NMR (300 MHz, $CDCl_3$) δ (ppm): 8.01 (s, ArH), 7.76-7.60 (br, ArH), 7.55-7.42 (br, ArH), 7.17-7.11 (br, ArH), 6.91-6.74 (br, ArH), 3.78 (br, O-$CH_2$), 1.67 (br, $CH_2$), 1.52-1.26 (br, $CH_2$), 0.91–0.87 (br, $CH_3$). Anal. Calcd (%) for $[(C_{41}H_{48}O_2)_{80}(C_{12}H_6O_2S)_{15}(C_{26}H_{30}N_2S_3)_5]_n$: C 83.93; H 8.01; N < 0.3; S 1.87. Found: C 83.70; H 8.38; N < 0.3; S 2.07.

PPF-SO15-DHTBT10:$^1$H NMR (300 MHz, $CDCl_3$) δ (ppm): 8.02 (s, ArH), 7.82-7.74 (br, ArH), 7.66-7.56 (br, ArH), 7.17-7.12 (br, ArH), 6.78 (br, ArH), 3.79 (br, O-$CH_2$), 1.68 (br, $CH_2$), 1.50-1.30 (br, $CH_2$), 0.91–0.87 (br, $CH_3$). Anal. Calcd (%) for $[(C_{41}H_{48}O_2)_{75}(C_{12}H_6O_2S)_{15}(C_{26}H_{30}N_2S_3)_{10}]_n$: C 83.04; H 7.91; N 0.55; S 2.84. Found: C 82.70; H 7.97; N 0.59; S 3.11.

$^1$H spectra were recorded on a Bruker DRX 300 spectrometer operating at 300 and 75 MHz in deuterated chloroform solution with tetramethylsilane as a reference. Gel permeation chromatography (GPC) measurements were performed in tetrahydrofuran (THF) with a Waters 2410 refractive-index detector. Three Waters Styragel columns HT3, HT4 and HT6 (all three 7.8 mm × 300 mm) were connected in series. The effective molecular weight ranges were 500–30 000 g/mol, 5000–600 000 g/mol, and 200 000–10 000 000 g/mol for Styragel column HT3, HT4 and HT6, respectively. Calibration was performed using the polystyrene kit SM-105 of 10 molecular weight standards from Shodex (Japan). The temperature of the columns was 35 °C, and the concentration for all the samples analyzed was 5 mg mL$^{-1}$. Cyclic voltammetry (CV) data were measured at a scan rate of 50 mV s$^{-1}$ at room temperature under argon using a CHI660A electro-chemical workstation with $Bu_4NPF_6$ (0.1 M) in acetonitrile as electrolyte. A platinum electrode coated with a thin polymer film was used as the working electrode and a Pt wire counter electrode and saturated calomel reference electrode completed the cell. Thermogravimetric analyses (TGA) were performed on a Netzsch TG 209 at a heating rate of 20 °C min$^{-1}$. The different scan calorimetry (DSC) were measured on a Netzsch DSC 204 under N2 flow at a heating rate of 10 °C min$^{-1}$. UV-vis absorption spectra were recorded with a HP 8453 spectrophotometer and photoluminescence (PL) spectra with a spectrofluorimeter (Spex Fluorolog-3). PL quantum yields were measured using an IS080 LabSphere integrating sphere with excitation by a 325 nm HeCd laser (Melles Griot).

*PLED Fabrication and Measurements*: The fabrication of the devices followed a well-established process. The ITO glass substrates with a sheet resistance of 15–20 ohm/square were cleaned in an ultrasonic bath successively in acetone, detergent, deionized water, and isopropanol. After oxygen plasma treatment, a 40 nm-thick PEDOT:PSS layer was spin-coated directly on the ITO substrate and dried by baking in a vacuum oven at 80 °C for 12 h. For some of the RGB PLEDs, a PVK layer (40 nm) was next spin-coated from chlorobenzene solution on top of the PEDOT:PSS. PPF-SO emission polymers were spin-coated on top of the PEDOT:PSS or PVK in chlorobenzene solution and PPF-SO15-BT and PPF-SO15-DHTBT polymers in p-xylene; all were then annealed at 100 °C on a hotplate for 20 min. For some of the PPF-SO15-DHTBT PLEDs a 30 nm thickness 2,2′,2′-(1,3,5-phenylene)-tris(1-phenyl-1H-benzimidazole) (TPBI) layer (thickness monitored with a STM-100/MF Sycon quartz crystal) was then thermally evaporated on top at a base pressure of 3.0 × 10$^{-4}$ Pa. For the WPLEDs, the emissive layer was spin-coated in chlorobenzene to form a uniform 80 nm thickness film on top of the PEDOT:PSS layer (no PVK was used), then annealed at 100 °C on a hotplate for 20 min. A 20 nm thickness PFN electron injection layer was spin-coated in methanol on top of the WPLED emissive layers (no TPBI was used) followed by drying inside a glovebox at 80 °C for 10 min. A Tencor Alpha-step 500 Surface Profilometer was used to determine the thicknesses of the polymer. Finally, 1.5 nm of CsF followed by 120 nm of aluminum (thickness monitored with a STM-100/MF Sycon quartz crystal) were thermally evaporated through a shadow mask at a base pressure of 3.0 × 10$^{-4}$ Pa to form the cathode. Overlap between the cathode and anode defined the 19 mm$^2$ pixel area. Except for deposition of the PEDOT:PSS layer from aqueous suspension, all other processes were carried out in the controlled atmosphere of a nitrogen dry-box (Vacuum Atmosphere Co.) containing less than 10 ppm oxygen and moisture. The current density-luminance-voltage (*J–L–V*) characteristics were measured in the nitrogen dry-box using a Keithley 236 source-measurement unit and a calibrated silicon photodiode. The electroluminescence spectra and CIE color coordinates were recorded using PR-705 SpectraScan spectrophotometer (Photo Research), while the corresponding color rendering index was calculated as described in the literature.[32] Atomic force microscopy (AFM) images were recorded in tapping mode on a Seiko SPA 400 equipped with an SPI 3800 probe station.

*ASE and Laser Characterization*: For gain measurements, planar waveguides were formed by spin-coating PPF-SO films in chlorobenzene solution of 20 mg/mL onto polished synthetic quartz substrates. The samples were optically pumped with a Q-switched, neodymium ion doped yttrium aluminum garnate [$Nd^{3+}$:YAG] laser pumped, optical parametric oscillator (OPO) that delivered 10 ns pulses at a 10 Hz repetition rate. The pump wavelength was chosen to match the absorption maximum of the polymers. The pulse energy incident on the sample was adjusted by insertion of calibrated neutral density filters into the beam path. The pump beam was focused with a cylindrical lens and spatially filtered through an adjustable slit to create a 400 μm × 4 mm excitation stripe on the sample. At sufficient excitation intensity, the spontaneously emitted photons that were waveguided along the stripe-shaped gain region were amplified via stimulated emission. This resulted in most of the light being emitted from the ends of the stripe. For this reason, one end of the stripe was aligned with the edge of the film and collected the emission with a fiber bundle placed nearby. The output from the fiber bundle was, in turn, focused into a grating spectrograph, wavelength dispersed and then detected with a charge-coupled device (CCD) detector. DFB lasers were fabricated by pre-patterning fued silica substrates with 1D surface grating structures (grating period $\Lambda$ = 290 nm, fill factor 50%, etch depth 90 nm) and then spin coating PPF-SO films on top. DFB lasers were optically pumped with the same OPO source used for ASE measurements and their emission was monitored with the same fiber-coupled spectrograph and CCD detector.

## Supporting Information

Supporting Information is available from the Wiley Online Library or from the author.

## Acknowledgements

L.Y. and J.L. contributed equally to this work. The authors are grateful for financial support from the National Natural Science Foundation of China (grant Nos. 21074038 and 51273069), State Key Basic Research Project of China (grant Nos. 2009CB623602 and 2009 CB930604) and the UK Engineering and Physical Sciences Research Council Collaborative Research Opportunities with China (Energy) programme (EP/F061757/1). D.D.C.B. is the Lee-Lucas Professor of Experimental Physics. R.X. is now at the Key Laboratory for Organic Electronics & Information Displays (KLOEID), Institute of Advanced Materials (IAM), Nanjing University of Posts and Telecommunications.

Received: December 12, 2012
Revised: January 28, 2013
Published online: April 2, 2013

[1] J. H. Burroughes, D. D. C. Bradley, A. R. Brown, R. N. Marks, K. D. Mackay, R. H. Friend, P. L. Burn, A. B. Holmes, *Nature* **1990**, *347*, 539.
[2] R. H. Friend, R. W. Gymer, A. B. Holmes, J. H. Burroughes, R. N. Marks, C. Taliani, D. D. C. Bradley, D. Dos Santos, J.-L. Brédas, M. Lögdlund, W. R. Salaneck, *Nature* **1999**, *397*, 121.
[3] B. W. D'Andrade, S. R. Forrest, *Adv. Mater.* **2004**, *16*, 1585.
[4] H. B. Wu, L. Ying, W. Yang, Y. Cao, *Chem. Soc. Rev.* **2009**, *38*, 3391.
[5] M. T. Bernius, M. Inbasekaran, J. O'Brien, W. Wu, *Adv. Mater.* **2000**, *12*, 1737.
[6] M. Campoy-Quiles, G. Heliotis, R. Xia, M. Ariu, M. Pintani, P. Etchegoin, D. D. C. Bradley, *Adv. Funct. Mater.* **2005**, *15*, 925.
[7] M. Gaal, E. J. W. List, U. Scherf, *Macromolecules* **2003**, *36*, 4236.
[8] M. Sims, D. D. C. Bradley, M. Ariu, M. Koeberg, A. Asimakis, M. Grell, D. G. Lidzey, *Adv. Funct. Mater.* **2004**, *14*, 765.
[9] F. Montiilla, R. Mallavia, *Adv. Funct. Mater.* **2007**, *17*, 71.
[10] D. Marsitzky, J. C. Scott, J. Chen, V. Y. Lee, R. D. Miller, S. Setayesh, K. Müllen, *Adv. Mater.* **2001**, *13*, 1096.

[11] J. Li, A. Ziegler, G. Wegner, *Chem. Eur. J.* **2005**, *11*, 4450.
[12] D. H. Hwang, M. J. Park, J. H. Lee, *Mater. Sci. Eng.* **2004**, *C24*, 201.
[13] T. H. Huang, W. T. Whang, J. Y. Shen, Y. S. Wen, J. T. Lin, T. H. Ke, L. Y. Chen, C. C. Wu, *Adv. Funct. Mater.* **2006**, *16*, 1449.
[14] J. A. Mikroyannidis, H. A. Moshopoulou, J. A. Anastassopoulos, M. M. Styllanakis, L. Fenenko, C. Adachi, *J. Polym. Sci. Part A: Polym. Chem.* **2006**, *44*, 6790.
[15] I. I. Perepichka, I. F. Perepichka, M. R. Bryce, I. O. Pålsson, *Chem. Commun.* **2005**, *27*, 3397.
[16] a) Y. Y. Li, H. B. Wu, J. H. Zou, L. Ying, W. Yang, Y. Cao, *Org. Electron.* **2009**, *10*, 901; b) J. Liu, S. J. Hu, W. Zhao, Q. H. Zou, W. Luo, W. Yang, J. B. Peng, Y. Cao, *Macromol. Rapid Commun.* **2010**, *31*, 496; c) L. Ying, Y. H. Xu, N. Li, J. A. Yang, Y. Y. Li, W. Yang, J. B. Peng, *J. Photon. Energy* **2012**, *2*, 021212; d) J. Liu, J. H. Zou, W. Yang, H. B. Wu, C. Liu, B. Zhang, J. B. Peng, Y. Cao, *Chem. Mater.* **2008**, *20*, 4499; e) H. P. Xiao, L. Yu, Y. H. Li, W. Yang, B. Zhang, W. Yang, H. B. Wu, Y. Cao, *Polymer* **2012**, *53*, 2873; f) L. Ying, Y. H. Li, C. H. Wei, M. Q. Wang, W. Yang, H. B. Wu, Y. Cao, *Chinese J. Polym. Sci.* **2013**, *31*, 88.
[17] E. P. Woo, M. Inbasekaran, W. R. Shiang, G. R. Roof, M. T. Bernius, W. Wu, US Patent 6,169,163, **1997**.
[18] C. I. Wilkinson, D. G. Lidzey, L. C. Palilis, R. B. Fletcher, S. J. Martin, X. H. Wang, D. D. C. Bradley, *Appl. Phys. Lett.* **2001**, *79*, 171.
[19] P. Herguth, X. Z. Jiang, M. S. Liu, A. K.-Y. Jen, *Macromolecules* **2002**, *35*, 6094.
[20] J. Liu, L. J. Bu, J. P. Dong, Q. G. Zhou, Y. H. Geng, D. G. Ma, L. X. Wang, X. B. Jing, F. S. Wang, *J. Mater. Chem.* **2007**, *17*, 2832.
[21] D.-Y. Chung, J. Huang, D. D. C. Bradley, A. J. Campbell, *Org. Electron.* **2010**, *11*, 1088.
[22] G. Heliotis, R. Xia, D. D. C. Bradley, G. A. Turnbull, I. D. W. Samuel, P. Andrew, W. L. Barnes, *J. Appl. Phys.* **2004**, *96*, 6959.
[23] H. Yoon, S. A. Maier, D. D. C. Bradley, P. N. Stavrinou, *Opt. Mater. Express* **2011**, *1*, 1127.
[24] N. Tokmoldin, N. Griffiths, D. D. C. Bradley, S. A. Haque, *Adv. Mater.* **2009**, *21*, 3475.
[25] Q. Hou, Q. M. Zhou, Y. Zhang, W. Yang, R. Q. Yang, Y. Cao, *Macromolecules* **2004**, *37*, 6299.
[26] J. H. Zou, H. Wu, H. B. Wu, W. C. H. Choy, J. B. Peng, Y. Cao, W.-Y. Wong, *Adv. Mater.* **2011**, *23*, 2976.
[27] B. H. Zhang, G. P. Tan, C.-S. Lam, Z. Y. Xie, W.-Y. Wong, J. Q. Ding, L. X. Wang, *Adv. Mater.* **2012**, *24*, **1873**.
[28] H. B. Wu, G. J. Zhou, J. H. Zou, C.-L. Ho, W.-Y. Wong, W. Yang, J. B. Peng, Y. Cao, *Adv. Mater.* **2009**, *21*, 4181.
[29] F. Huang, P.-I. Shih, C.-F. Shu, Y. Chi, A. K.-Y. Jen, *Adv. Mater.* **2009**, *21*, 361.
[30] Y. H. Xu, J. B. Peng, Y. Q. Mo, Q. Hou, Y. Cao, *Appl. Phys. Lett.* **2005**, *86*, 163502.
[31] X. Gong, S. Wang, D. Moses, G. C. Bazan, A. J. Heeger, *Adv. Mater.* **2005**, *17*, 2053.
[32] J. H. Zou, J. Liu, H. B. Wu, J. B. Peng, W. Yang, Y. Cao, *Org. Electron.* **2009**, *10*, 843.
[33] J. Liu, Q. G. Zhou, Y. X. Cheng, Y. H. Geng, L. X. Wang, D. G. Ma, X. B. Jing, F. S. Wang, *Adv. Funct. Mater.* **2006**, *16*, 957.
[34] Q. J. Sun, B. H. Fan, Z. A. Tan, C. H. Yang, Y. F. Li, Y. Yang, *Appl. Phys. Lett.* **2006**, *88*, 163510.
[35] C. Belton, G. Itskos, G. Heliotis, P. N. Stavrinou, P. G. Lagoudakis, J. Lupton, S. Pereira, E. Gu, C. Griffin, B. Guilhabert, I. M. Watson, A. R. Mackintosh, R. A. Pethrick, J. Feldmann, R. Murray, M. D. Dawson, D. D. C. Bradley, *J. Phys. D: Appl. Phys.* **2008**, *41*, 094006.
[36] Q. L. Niu, Y. H. Xu, J. X. Jiang, J. B. Peng, Y. Cao, *J. Lumin.* **2007**, *126*, 531.
[37] J. S. Huang, G. Li, E. Wu, Q. F. Xu, Y. Yang, *Adv. Mater.* **2006**, *18*, 114.
[38] P.-I. Shih, Y.-H. Tseng, F.-I. Wu, A. K. Dixit, C.-F. Shu, *Adv. Funct. Mater.* **2006**, *16*, 1582.
[39] S. H. Kim, Y. Jin, J. Y. Yu, J. Kim, S. Song, H. Suh, K. Lee, *Synth. Met.* **2010**, *160*, 835.
[40] C. R. Belton, A. L. Kanibolotsky, J. Kirkpatrick, C. Orofino, S. E. T. Elmasly, P. N. Stavrinou, P. J. Skabara, D. D. C. Bradley, *Adv. Funct. Mater.* DOI: 10.1002/adfm.201202644.
[41] R. D. Xia, G. Heliotis, Y. B. Hou, D. D. C. Bradley, *Org. Electron.* **2003**, *4*, 165.
[42] L. J. Zhang, S. J. Hu, J. W. Chen, Z. H. Chen, H. B. Wu, J. B. Peng, Y. Cao, *Adv. Funct. Mater.* **2011**, *21*, 3760.
[43] T. Forster, *Discuss. Faraday Soc.* **1959**, *7*, 27.
[44] T. Virgili, D. G. Lidzey, D. D. C. Bradley, *Adv. Mater.* **2000**, *12*, 58.
[45] B. K. Yap, R. D. Xia, M. Campoy-Quiles, P. N. Stavrinou, D. D. C. Bradley, *Nat. Mater.* **2008**, *7*, 376.
[46] R. Xia, G. Heliotis, D. D. C. Bradley, *Appl. Phys. Lett.* **2003**, *82*, 3599.
[47] R. D. Xia, G. Heliotis, M. Campoy-Quiles, P. N. Stavrinou, D. D. C. Bradley, D. Vak, D. Kim, *J. Appl. Phys.* **2005**, *98*, 083101.
[48] G. Heliotis, S. A. Choulis, G. Itskos, R. Xia, R. Murray, P. N. Stavrinou, D. D. C. Bradley, *Appl. Phys. Lett.* **2006**, *88*, 081104.
[49] Q. Hou, Y. S. Xu, W. Yang, M. Yuan, J. B. Peng, Y. Cao, *J. Mater. Chem.* **2002**, *12*, 2887.
[50] R. Xia, P. N. Stavrinou, D. D. C. Bradley, Y. Kim, *J. Appl. Phys.* **2012**, *111*, 123107.
[51] J. L. Brédas, R. Silbey, D. S. Boudreaux, R. R. Chance, *J. Am. Chem. Soc.* **1983**, *105*, 6555.
[52] L. D. Hou, L. Duan, J. Qiao, D. Q. Zhang, G. F. Dong, L. D. Wang, Y. Qiu, *Org. Electron.* **2010**, *11*, 1344.
[53] M. D. McGehee, A. J. Heeger, *Adv. Mater.* **2000**, *12*, 1655.
[54] M. Sims, K. Zheng, M. Campoy-Quiles, R. Xia, P. N. Stavrinou, D. D. C. Bradley, P. Etchegoin, *J. Phys. Condens. Matter.* **2005**, *17*, 6307.
[55] R. D. Xia, W.-Y. Lai, P. A. Levermore, W. Huang, D. D. C. Bradley, *Adv. Funct. Mater.* **2009**, *19*, 2844.
[56] W.-Y. Lai, R. D. Xia, Q.-Y. He, P. A. Levermore, W. Huang, D. D. C. Bradley, *Adv. Mater.* **2009**, *21*, 355.
[57] R. Xia, G. Heliotis, P. N. Stavrinou, D. D. C. Bradley, *Appl. Phys. Lett.* **2005**, *87*, 031104.
[58] H. B. Wu, F. Huang, Y. Q. Mo, W. Yang, D. L. Wang, J. B. Peng, Y. Cao, *Adv. Mater.* **2004**, *16*, 1826.
[59] F. Huang, H. B. Wu, D. L. Wang, W. Yang, Y. Cao, *Chem. Mater.* **2004**, *16*, 708.
[60] M. C. Gather, R. Alle, H. Becker, K. Meerholz, *Adv. Mater.* **2007**, *19*, 4460.
[61] R. W. G. Hunt, *Measuring Color*, 2nd ed. Ellis Horwood, Hemel Hempstead, UK **1991**, pp. 38–109.
[62] F.-C. Chen, S.-C. Chang, G. He, S. Pyo, Y. Yang, M. Kurotaki, J. Kido, *J. Polym. Sci. Part B: Polym. Phys.* **2003**, *41*, 2681.
[63] E. B. Namdas, A. Ruseckas, I. D. W. Samuel, S.-C. Lo, P. L. Burn, *J. Phys. Chem.* **2004**, *108*, 1570.
[64] S. Q. Fan, M. L. Sun, J. Wang, W. Yang, Y. Cao, *Appl. Phys. Lett.* **2007**, *91*, 213502.